Neurophotonics

Neurophotonics.SPIEDigitalLibrary.org

Semiautomated segmentation and analysis of retinal layers in three-dimensional spectral-domain optical coherence tomography images of patients with atrophic age-related macular degeneration

Zhihong Hu
Yue Shi
Kiran Nandanan
Srinivas R. Sadda
APGS Study Group

SPIE.

Zhihong Hu, Yue Shi, Kiran Nandanan, Srinivas R. Sadda, APGS Study Group, "Semiautomated segmentation and analysis of retinal layers in three-dimensional spectral-domain optical coherence tomography images of patients with atrophic age-related macular degeneration," *Neurophoton.* **4**(1), 011012 (2017), doi: 10.1117/1.NPh.4.1.011012.

Semiautomated segmentation and analysis of retinal layers in three-dimensional spectral-domain optical coherence tomography images of patients with atrophic age-related macular degeneration

Zhihong Hu,[a] Yue Shi,[a] Kiran Nandanan,[a] Srinivas R. Sadda,[a,b,*] and APGS Study Group[c]
[a]Doheny Eye Institute, Los Angeles, California, United States
[b]David Geffen School of Medicine at UCLA, Department of Ophthalmology, Los Angeles, California, United States
[c]Beckman AMD Phenotype Genotype Study (APGS) Group, Los Angeles, California, United States

Abstract. Historically, regular drusen and geographic atrophy (GA) have been recognized as the hallmarks of nonneovascular age-related macular degeneration (AMD). Recent imaging developments have revealed another distinct nonneovascular AMD phenotype, reticular pseudodrusen (RPD). We develop an approach to semiautomatically quantify retinal surfaces associated with various AMD lesions (i.e., regular drusen, RPD, and GA) in spectral domain (SD) optical coherence tomography (OCT) images. More specifically, a graph-based algorithm was used to segment multiple retinal layers in SD-OCT volumes. Varying surface feasibility constraints based on the presegmentation were applied on the double-surface graph search to refine the surface segmentation. The thicknesses of these layers and their correlation with retinal functional measurements, including microperimetry (MP) sensitivity and visual acuity (VA), were investigated. The photoreceptor outer segment layer demonstrated significant thinning with a reduction in MP sensitivity and VA score when atrophic AMD lesions were present. Regular drusen and RPD were separately segmented on SD-OCT images to allow their characteristics and distribution to be studied separately. The mean thickness of regular drusen was found to significantly correlate with the VA score. RPD appeared to be distributed evenly throughout the macula and regular drusen appeared to be more concentrated centrally. [DOI: 10.1117/1.NPh.4.1.011012]

Keywords: semiautomated segmentation and analysis; retinal layers; spectral optical coherence tomography images; atrophic age-related macular degeneration.

Paper 16038SSRRR received Jun. 8, 2016; accepted for publication Jan. 12, 2017; published online Feb. 6, 2017.

1 Introduction

Spectral-domain optical coherence tomography (SD-OCT) is a three-dimensional (3-D), *in vivo* imaging technique that permits direct visualization of retinal morphology and architecture.[1] In the setting of retinal or optic nerve disease, the retinal layer thickness may be affected either locally or globally, depending on the specific disease. In terms of vision and blindness in the United States, the three most important diseases are age-related macular degeneration (AMD), diabetic retinopathy, and glaucoma.[2–4] The identification of the retinal layers and the quantification of their layer-specific properties may facilitate our understanding of the pathogenesis and evolution of various retinal diseases.

AMD is the leading cause of blindness in people aged 65 and older in the western world.[5] It may present extracellular abnormal deposits associated with neuronal degeneration, drusen, and neovascular membranes, respectively. Historically, regular drusen and geographic atrophy (GA) have been recognized as the hallmarks of atrophic AMD. With its characteristic loss of the retinal pigment epithelium (RPE) and photoreceptors, GA is a manifestation of advanced or late AMD.[6,7] Regions of GA in OCT scans demonstrate thinning of the hyper-reflective external band, corresponding to attenuation of the RPE/Bruch's membrane (BM) complex and increased transmission of signal to the deeper choroid as a result of the loss of outer layers, including photoreceptors. Regular drusen are the most common early sign of dry AMD. These deposits show up as tiny yellow or white deposits at the level of BM on the color fundus images, but they are visualized more easily by SD-OCT.

Several studies have emphasized the importance of large drusen[8–10] in early and intermediate AMD. Developments in imaging over the past decade have revealed that a further distinct phenotype, reticular pseudodrusen (RPD), or reticular drusen are strongly associated with the development of late AMD. RPD, which appear as yellowish interlacing networks in color fundus images, are also better visualized using infrared imaging, blue light fundus autofluorescence, or SD-OCT. Studies correlating SD-OCT and confocal scanning laser ophthalmoscopy have shown that RPD appear to correspond to subretinal deposits, located internal to the RPE, in contrast to traditional drusen, which are located external to the RPE.[11] As multiple longitudinal studies have revealed that RPD are strong predictors for progression to GA,[11–15] interest in understanding the role that RPD play in the pathogenesis of AMD has grown.

*Address all correspondence to: Srinivas R. Sadda, E-mail: ssadda@doheny.org

In areas of GA, OCT images demonstrate thinning of the retina/RPE complex, while they are thicker than normal in areas of regular drusen and/or RPD. Quantitative analysis of retinal layer thickness associated with these distinct AMD phenotypes is important for understanding the progression of AMD. Manual tracing of the multiple retinal layers in volumetric SD-OCT images is tedious and time-consuming. While a system for automatically detecting the multiple retinal layers is attractive, automated detection is not a trivial undertaking because of the complexity of the layer structures and the disturbances produced by the eye diseases. We and others[16–19] have applied a graph search framework to facilitate automated multiple retinal layer segmentation in SD-OCT volumes, demonstrating suitability for several applications. Based on the graph search framework, we have semiautomatically segmented regular drusen in SD-OCT images.[20] Semiautomated and automated regular drusen segmentation have also been reported by other groups;[21,22] however, to the best of our knowledge, there are no reported approaches to identify RPD in SD-OCT images either semiautomatically or automatically.

Microperimetry (MP) and visual acuity (VA) are two typical tools for retinal functional measurements.[23] Quantitative analysis of the relationship of the structural parameters (retinal thickness) with the functional measurements may be helpful for understanding the progression of atrophic AMD. Thus, as a preliminary investigation, we describe a semiautomated graph-based multilayer approach to segmenting retinal surfaces associated with atrophic AMD. The relationship between the thicknesses of these layers and retinal functional measurements (MP sensitivity and VA) is also investigated.

2 Materials

2.1 *Subject Recruitment*

Forty-five eyes from 41 subjects were identified as part of the Beckman AMD Phenotype Genotype Study (APGS). These included both control eyes and eyes with atrophic AMD. All subjects provided written informed consent. The study was approved by the Institutional Review Board of University of California, Los Angeles and adhered to the tenets set forth in the Declaration of Helsinki.

2.2 *Imaging*

For structural measurements of retinal layers, each subject underwent volume OCT imaging using a Heidelberg Spectralis (Heidelberg Engineering, Heidelberg, Germany) SD-OCT. All volume scans consisted of macular cube scan patterns. The image dimensions and physical dimensions varied slightly among cases. On average, the image scan dimensions are $496\,(\text{depth}) \times 1084\,(\text{A scans}) \times 53\,(\text{B-scans})$ voxels and the physical dimensions are $1.92\,\text{mm}\,(\text{depth}) \times 6.80\,\text{mm}\,(\text{A scans}) \times 6.41\,\text{mm}\,(\text{B-scans})$. The voxel depth was 8 bits in grayscale. To provide consistency for the quantitative analysis of the retinal layer properties among different volume scans, all the right eye scans were horizontally flipped in the x-direction.

In addition, MP sensitivity (mesopic MP-1) from centervue macular integrity assessment (MAIA) (CenterVue Inc., San Jose, California) and best-corrected VA scores [number of letters on early treatment of diabetic retinopathy (ETDRS) charts] were used for the functional measurements, with fields flipped as appropriate to match the OCTs.

3 Methods

3.1 *Overview*

Our surface segmentation overall used a double-surface graph search segmentation approach[16–20] to perform an initial surface segmentation, which simultaneously identified the internal limiting membrane (ILM) and ellipsoid zone (EZ), as well as the photoreceptor outer segment (OS) (outer border) and outer RPE, respectively. In the initial surface segmentation, constant surface feasibility constraints based on observation were applied for all surfaces. To achieve better segmentation of the photoreceptor OS (outer border) and outer RPE, varying surface feasibility constraints based on the presegmentation were applied on the double-surface graph search utilized to refine the surface segmentation.

3.2 *Segmentation of Multiple Retinal Surfaces*

The graph search approach used in this study was an evolution of the strategy previously described by Li et al.[16] The segmentation of multiple surfaces could be considered as an optimization problem with the goal being to find a set of surfaces with the minimum cost such that the found surface set was feasible. To find a set of surfaces with the minimum cost, a graph with a subset of graphs corresponding to each individual surface was constructed. The cost function was a signed edge-based term, favoring a dark-to-bright or bright-to-dark intensity transition based on different surfaces. Surface feasibility constraints, i.e., smoothness constraints within a particular surface and interaction constraints between different surfaces, were applied to limit the neighborhood search. Thus, the smoothness constraints and the interaction constraints played an important role in accurately segmenting the multiple layers.

In the previous approach of Li et al.,[16] both the smoothness and interaction constraints were of a constant value. In this study, for the initial surface segmentation of the ILM, EZ, photoreceptor OS (outer border), and the outer RPE, constant surface feasibility constraints based on observation were applied on both the smoothness and interaction constraints. However, in the refined surface segmentation of the photoreceptor OS (outer border) and outer RPE, varying smoothness and interaction constraints were applied. More specifically, for example, for the smoothness constraints in the x-direction for both the refined photoreceptor OS (outer border) and outer RPE, considering two neighboring graph columns $\{(x_1, y_1), (x_1 + 1, y_1)\}$, when moving from column (x_1, y_1) to column $(x_1 + 1, y_1)$, assuming a normal distribution and allowing for 99.7% of the expected changes in z-value (which lie within three standard deviations 3σ),[24] the smoothness constraints in the x-direction are enforced to define the allowed change of the surface height to the lower ($\Delta^l_{\{(x_1,y_1),(x_{1+1},y_1)\}}$) or upper ($\Delta^u_{\{(x_1,y_1),(x_{1+1},y_1)\}}$) position

$$\Delta^l_{\{(x_1,y_1),(x_{1+1},y_1)\}} = \mu + 3.0 * \sigma$$

$$\Delta^u_{\{(x_1,y_1),(x_{1+1},y_1)\}} = -(\mu - 3.0 * \sigma),$$

where μ was the mean deviation of $\{f(x_1, y_1) - f(x_1 + 1, y_1)\}$ from the initial segmented surface and σ was the absolute of the deviation of the segmented surface subtracting the mean deviation. The smoothness constraints in the y-direction were set similarly.

For the interaction constraints between the refined photoreceptor OS (outer border) and the outer RPE, the minimum

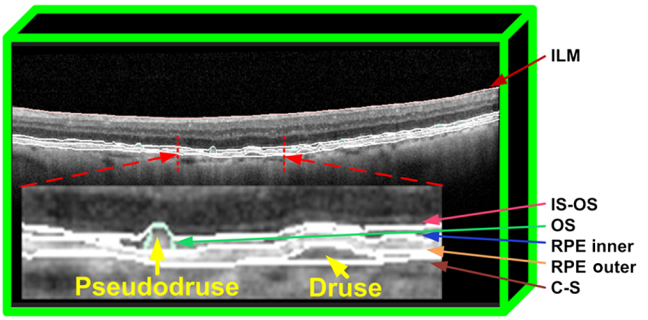

Fig. 1 Illustration of the multiple layer segmentation, including the RPD and regular drusen layers.

allowed distance between the two surfaces at each column was set as the mean thickness minus 3.0 times the absolute value of the thickness of the presegmented photoreceptor OS (outer border) and the outer RPE at that column, subtracting the mean thickness. The maximum allowed distance between the two surfaces at each column was set as the mean thickness plus 3.0 times the absolute value of the thickness of the presegmented photoreceptor OS (outer border) and the outer RPE at that column, subtracting the mean thickness.

Based on the segmented photoreceptor OS (outer border) and outer RPE, additional fitting was performed at the positions of pseudodrusen and regular drusen to define the inner RPE and inner choroid boundaries. The pseudodrusen were located at the layer between the photoreceptor OS (outer border) and inner RPE. Regular drusen were located at the layer between the outer RPE and inner choroid. In total, the segmentation resulted in four retinal sublayers: namely the OSs, RPD, RPE, and regular drusen layers. Figure 1 shows an illustration of the segmented retinal layers.

3.3 *Experimental Methods*

In this study, the thicknesses of the four retinal layers were quantitatively evaluated. Accurate quantitative analysis of retinal layer thickness was highly dependent on accurate surface segmentation. To achieve accurate layer thickness analysis, automated segmentation was manually corrected by a certified grader (YS) as needed and reviewed by reading center medical director (SS).

For statistical analysis, any eyes having OCT images, corresponding MP, and VA measurements were included. Eyes with evidence of neovascular AMD (NVAMD) were excluded. In total, 45 eyes were included in this study for quantitative analysis. Functional (MP sensitivity and VA score) and structural (retinal layer thickness) correlation based on each individual eye were investigated within the regions with diameters of 3 mm (referred as $D = 3$ mm region) and 5 mm (referred as $D = 5$ mm region) relative to the foveal center. In addition, the 45 eyes were divided into four groups: CTRL group (13 eyes), drusen only group (13 eyes), drusen + RPD group (14 eyes), and GA (+ drusen + RPD) group (5 eyes). The criteria of the division of the different groups were as follows:

- CTRL group:
  - ✓ eyes without GA
  - ✓ RPD volume < 0.01 mm^3, if any
  - ✓ Drusen volume < 0.03 mm^3, if any
- Drusen only group: eyes with only drusen (volume ≥ 0.03 mm^3)
- Drusen + RPD group: eyes with RPD (volume ≥ 0.01 mm^3)
- GA group: eyes with definite GA

Pearson's coefficient r was used to evaluate the structure–function correlation for all the eyes and for eyes in different groups. Multiple regression analysis of MP sensitivity and VA versus retinal layer thickness was performed to test for significant associations. An alpha level of $P < 0.05$ was chosen as the criterion of significance.

4 Results

The results of the thicknesses of the segmented retinal layers and their correlations with the retinal functional measurements (MP sensitivities and VA scores) were investigated by five experiments as described below.

4.1 *Experiment 1: Structure–Function Multiple Regression Analysis*

In experiment 1, considering all 45 eyes, using the mean thicknesses of OS, RPD, RPE, and regular drusen as independent variables and using MP sensitivity and VA score as dependent variables, the multiple linear regression analysis was performed to identify the significant predictors of the MP sensitivity and VA score. Of note, other investigators have combined the RPD, RPE, and regular drusen layers (termed RPEDC, RPE/drusen complex).[8] To allow comparison to these previous studies, the RPEDC complex was also included in the multiple linear regression analysis. Considering these five layers (OS, RPD, RPE, regular drusen, and RPEDC), only the thickness of the OS layer was found to be a significant predictor of vision and remained in the final model as shown in Table 1.

Furthermore, as shown in Fig. 2, the OS layer thicknesses were compared among the four groups (CTRL, drusen only, drusen + RPD, and GA) and demonstrated a trend for reduction with more advanced disease, considering RPD to be the evidence of worse disease compared to drusen alone.

4.2 *Experiment 2: Structure–Function Correlation*

In experiment 2, structure–function correlations between the mean MP sensitivity and mean VA score with the thicknesses of OS, RPD, RPE, regular drusen, and RPEDC complex layers in $D = 3$ mm and $D = 5$ mm regions for all the 45 eyes were investigated, respectively. Table 2 shows the correlations of mean MP sensitivities and different layer thicknesses for all

Table 1 Multiple regression analysis of function–structure correlation in $D = 5$ mm region for all 45 eyes.

	Overall model		Significant predictors	
Dependent variables	R^2	P-value	Layer	P-value
MP sensitivity	0.40	<0.05	OS	<0.05
VA score	0.25	<0.05	OS	<0.05

MP, microperimetry; VA, visual acuity; OS, outer segment.

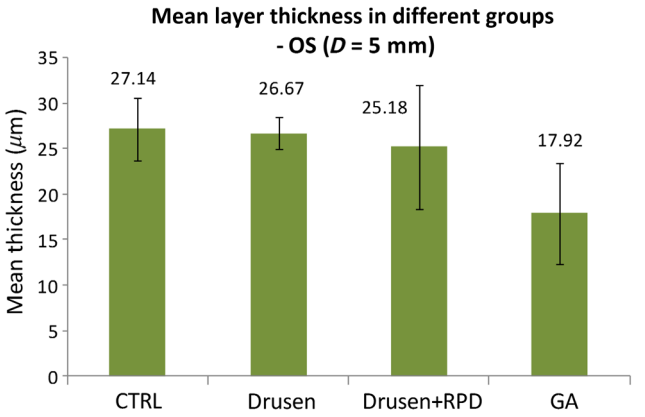

Fig. 2 Comparison of mean OS layer thickness in different groups.

the 45 eyes, and Table 3 shows those of mean VA scores and different layer thicknesses for all 45 eyes. As Table 2 shows, when all 45 eyes are considered, in both regions of $D = 3$ mm and $D = 5$ mm, lower MP sensitivity was associated with thinner OS and thinner RPE. The mean thicknesses of RPD and drusen within 3 mm did not correlate with MP sensitivities (nor did the combined RPEDC), whereas the mean thickness of drusen within 5 mm had a weak correlation with MP. Table 3 shows the results of a similar experiment of structure–function correlations between the VA score and retinal layer thickness. When all 45 eyes are considered, a lower VA score was associated with thinner OS in both regions of $D = 3$ mm and $D = 5$ mm. The mean thickness of RPD did not correlate with VA score. However, the mean thickness of regular drusen in both regions and that of RPEDC within 3 mm significantly correlated with VA scores, whereas there was no correlation between the mean thickness of RPEDC and VA score within 5 mm.

4.3 *Experiment 3: Function–Function Correlation*

Experiment 3 investigated the function–function correlation of the mean MP sensitivity and mean VA for all the 45 eyes. The correlation of the mean MP sensitivity and mean VA for this cohort as a whole was $r = 0.08$ ($P = 0.59$), which was not statistically significant. When considered by groups of CTRL, drusen only, drusen + RPD, and GA, both the mean MP sensitivity and mean VA score again showed a trend of decreasing with more advanced disease (Fig. 3).

4.4 *Experiment 4: Structure–Function Correlation in Drusen + RPD Group*

To better understand the structure–function measurements in the presence of RPD, experiment 4 focused on the analysis of the drusen + RPD group alone. In experiment 4, the 14 eyes in the drusen + RPD group were divided into two subgroups, sorted by MP sensitivity. The mean MP sensitivity and mean thickness were compared in different layers of the two groups in $D = 5$ mm. As shown in Table 4, an unpaired t-test between the two groups indicated that significant thinning of the OS layer was observed in eyes with the worse MP sensitivity (note that the distinct retinal layers' thickness and MP sensitivity of the two groups were provided in the Table 5). The RPD, drusen, and RPEDC layers were thickened but the differences were not statistically significant. Additionally, the mean MP sensitivity and mean thickness in $D = 3$ mm region were also compared for the different layers between the two groups. However, no significant difference was found.

Table 2 Correlation of mean MP sensitivity versus mean layer thickness for all 45 eyes.

Layer	Diameter (mm)	Pearson's r	P-value
OS	$D = 3$	0.66	<0.001
	$D = 5$	0.53	<0.001
RPD	$D = 3$	−0.16	0.31
	$D = 5$	−0.22	0.15
RPE	$D = 3$	0.60	<0.001
	$D = 5$	0.37	<0.01
Drusen	$D = 3$	−0.12	0.44
	$D = 5$	−0.32	<0.05
RPEDC	$D = 3$	0.17	0.28
	$D = 5$	−0.17	0.28

OS, outer segment; RPD, reticular pseudodrusen; RPE, retinal pigment epithelium; RPEDC, RPE and drusen complex.

Table 3 Correlation of VA score versus mean layer thickness for all 45 eyes.

Layer	Diameter (mm)	Pearson's r	P-value
OS	$D = 3$	0.39	<0.01
	$D = 5$	0.33	<0.05
RPD	$D = 3$	0.04	0.79
	$D = 5$	−0.08	0.60
RPE	$D = 3$	0.05	0.75
	$D = 5$	0.16	0.29
Drusen	$D = 3$	−0.45	<0.05
	$D = 5$	−0.37	<0.05
RPEDC	$D = 3$	−0.39	<0.01
	$D = 5$	−0.27	0.08

OS, outer segment; RPD, reticular pseudodrusen; RPE, retinal pigment epithelium; RPEDC, RPE and drusen complex.

4.5 *Experiment 5: Regional Thickness Comparison in Drusen + RPD Group*

In experiment 5, the RPD and regular drusen layer thicknesses in the drusen + RPD group in the $D = 3$ mm and $D = 5$ mm regions were compared. As shown in Fig. 4, RPD appeared to be distributed evenly throughout the macula, with similar thicknesses in the central 3-and 5-mm circles. Regular drusen, in contrast, appeared to be thicker centrally, with a greater

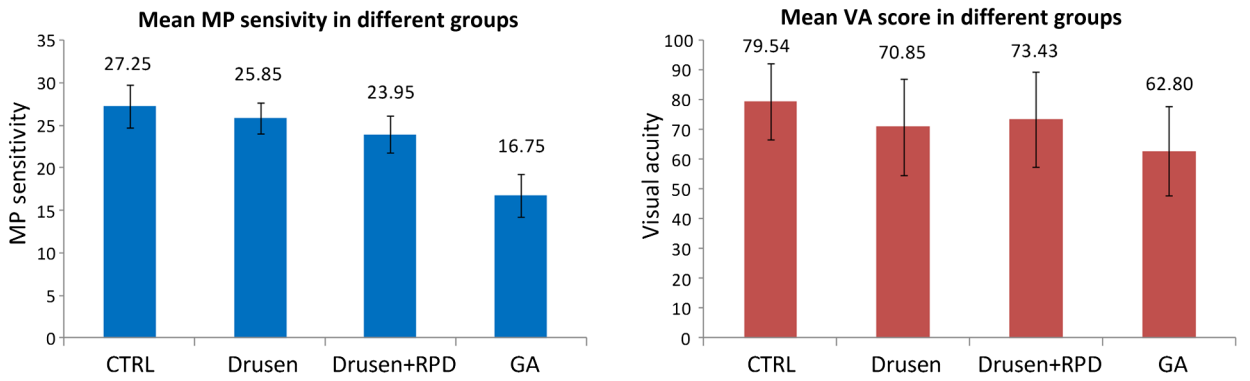

Fig. 3 Comparison of mean MP sensitivity and mean VA score in different groups.

Table 4 Mean layer thickness versus MP sensitivity in drusen + RPD subgroup in $D = 5$ mm region.

		Layer thickness (μm)				
Group	MP sensitivity	OS	RPD	RPE	Drusen	RPEDC
Group 1 (7 eyes)	22.2 ± 1.42	21.47 ± 1.35	5.29 ± 4.66	30.56 ± 3.05	7.04 ± 10.69	43.87 ± 8.59
Group 2 (7 eyes)	25.69 ± 0.98	28.89 ± 8.01	2.75 ± 2.58	29.32 ± 2.36	5.52 ± 3.25	37.52 ± 4.86
P-value*	<0.001	<0.05	0.24	0.41	0.73	0.12

MP, microperimtry; OS, outer segment; RPD, reticular pseudodrusen; RPE, retinal pigment epithelium; RPEDC, RPE and drusen complex.
**P*-value of the unpaired *t*-test of the two groups.

thickness in the central 3-mm circle. The combined RPEDC layer shows a regional distribution similar to that of regular drusen, suggesting that drusen are the largest contributor to this combined layer.

5 Discussion and Conclusion

In this study, a semiautomated, graph-based, multilayer approach was developed to segment multiple retinal layers (OS, RPD, RPE, and regular drusen) relevant to atrophic AMD. The thicknesses of these layers and their correlations with retinal functional measurements (MP sensitivities and VA scores) were investigated by five experiments.

Although there have been many studies characterizing the phenotype of atropgic AMD;[13,25–28] and although we and other groups have also developed algorithms for the segmentation of atrophic AMD lesions,[20–22] so far, there have been no reports of algorithms for segmentation of RPD, RPE, and regular drusen separately. In this study, we first showed that regular drusen and RPD can be separately segmented on SD-OCT images to allow the distribution and progression of these lesions to be studied separately. Additionally, the thinning of the OS layer was observed to strongly associate with the loss of the MP sensitivity and VA score with the presence of atrophic AMD lesions. This observation makes sense, as the OSs would be expected to be required for phototransduction and vision. Also of note, considering the entire cohort, the mean thickness of RPD did not correlate well with the MP sensitivity, nor with the VA score. This is not surprising, since it is well known that RPD undergo an evolution over time,[29] with an initial increase and coalescence of RPD followed by a slow disappearance of RPD along with the OS. Thus, the RPD in the early stage can be quite thin and associated with good function and in the late phase as the RPD disappear, they can again be reduced in thickness, but now with loss of the OS and poor vision.

Interestingly, the mean thickness of regular drusen demonstrated statistically significant correlation with the VA score. It should be noted that whereas RPD appeared to be distributed evenly throughout the macula, regular drusen appeared to be thicker centrally. Thus, given the central location, one might expect regular drusen to preferentially disrupt the function of foveal photoreceptors, and thus have an impact on VA.

We compared the RPEDC thicknesses with the presence of AMD in our dataset and that in the dataset of Ref. 8. In our dataset, the mean RPEDC thickness within $D = 5$ mm was 29.94 ± 2.70 μm, while in Ref. 8, it was 35.08 ± 11.8 μm. Although the two datasets are different, their RPEDC thicknesses are at the same level, considering their standard deviations.

It needs to be pointed out that regarding the validation of the layer segmentation with drusen, we have published a paper.[20] For pseudodrusen segmentation, the performance is not ideal at this stage. We are developing a fully automated multimodal segmentation approach which allows the identification of RPD and drusen on 2-D en-face OCT images and fundus images first. By using the presegmented RPD and drusen information, we expect the layer segmentation of RPD will be enhanced and the validation would be included then. For this paper, as the heavy manual correction (about 50%) was performed for the analysis, we referred to our current layer segmentation as the semiautomated approach as can be seen in the title.

Regarding the correlation of focal lesions with MP values as shown in Table 2, the drusen layer was correlated with MP for the $D = 5$ mm region but not the $D = 3$ mm region which might be contradictory to our expectation as the drusen

Table 5 Mean layer thickness and mean MP sensitivity in drusen + RPD subgroup in $D = 5$ mm region.

		Layer thickness (μm)				
Group	MP sensitivity	OS	RPD	RPE	Drusen	RPEDC
Group 1 (7 eyes)	19.54	20.88	4.32	30.69	6.17	41.07
	21.43	23.41	0.67	29.87	29.74	60.28
	22.00	21.73	1.36	31.48	0.05	32.89
	22.49	19.92	4.85	35.85	2.99	42.47
	23.05	20.14	11.91	26.92	0.31	39.85
	23.14	21.17	11.61	27.21	0.00	41.84
	23.87	23.04	2.31	31.93	10.01	48.69
Mean ± STD	22.2 ± 1.42	21.47 ± 1.35	5.29 ± 4.66	30.56 ± 3.05	7.04 ± 10.69	43.87 ± 8.59
Group 2 (7 eyes)	24.51	38.82	0.63	32.18	5.19	38.00
	24.70	38.20	0.98	27.19	4.01	32.18
	25.14	23.34	6.77	29.07	8.41	44.26
	25.84	35.35	0.77	26.86	7.98	35.11
	25.94	21.94	6.07	27.23	1.15	34.44
	26.50	22.76	2.11	32.35	9.63	44.10
	27.22	21.80	1.88	30.38	2.29	34.55
Mean ± STD	25.69 ± 0.98	28.89 ± 8.01	2.75 ± 2.58	29.32 ± 2.36	5.52 ± 3.25	37.52 ± 4.86

MP, microperimetry; OS, outer segment; RPD, reticular pseudodrusen; RPE, retinal pigment epithelium; RPEDC, RPE and drusen complex.
*P-value of the unpaired t-test of the two groups.

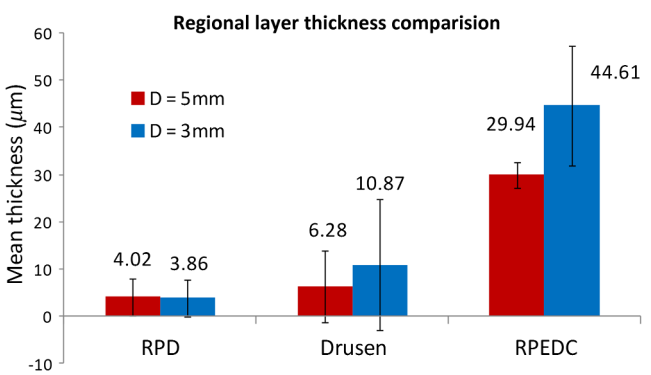

Fig. 4 Regional thickness comparison in Drusen + RPD group.

distributed more centrally. One of the MP patterns used in this study was condensed around foveal center (within about 3 mm). However, the image B-scans were sparse in this dataset with an average of 53 over 6.41 mm. Although the linear interpolation was performed in the OCT images and segmentation, it might not reflect the real topology of the retina, and further might not reflect the real structure–function correlation, especially for the region within 3 mm. OCT images with denser B-scans are preferred in the future studies.

In conclusion, in this study, a semiautomated graph-based multilayer approach was developed to segment retinal surfaces associated with atrophic AMD. Regular drusen and RPD were separately segmented on SD-OCT images to allow the distribution and progression of these lesions to be studied separately.

Disclosures

No conflicts of interest, financial or otherwise, are declared by the authors.

Acknowledgments

This work was supported in part by the Macula Vision Research Foundation, the Beckman Macular Degeneration Research Center, the Beckman AMD Phenotype Genotype Study (APGS) Group, and a Research to Prevent Blindness Physician Scientist Award.

References

1. W. Drexler and J. G. Fujimoto, "State-of-the-art retinal optical coherence tomography," *Prog. Retinal Eye Res.* **27**, 45–88 (2008).
2. C. K. Leung et al., "Retinal nerve fiber layer imaging with spectral-domain optical coherence tomography: patterns of retinal nerve fiber layer progression," *Ophthalmology* **119**, 1858–1866 (2012).
3. S. E. Chung et al., "Choroidal thickness in polypoidal choroidal vasculopathy and exudative age-related macular degeneration," *Ophthalmology* **118**, 840–845 (2011).

4. M. A. Sandberg et al., "Visual acuity is related to parafoveal retinal thickness in patients with retinitis pigmentosa and macular cysts," *Invest. Ophthalmol. Vis. Sci.* **49**, 4568–4572 (2008).
5. R. Klein et al., "Changes in visual acuity in a population over a 15 year period: the Beaver Dam eye study," *Am. J. Ophthalmol.* **142**, 539–549 (2006).
6. C. J. Blair, "Geographic atrophy of the retinal pigment epithelium. A manifestation of senile macular degeneration," *Arch. Ophthalmol.* **93**, 19–25 (1975).
7. J. P. Sarks, S. H. Sarks, and M. C. Killingsworth, "Evolution of geographic atrophy of the retinal pigment epithelium," *Eye* **2**, 552–577 (1988).
8. S. Farsiu et al., "Quantitative classification of eyes with and without intermediate age-related macular degeneration using optical coherence tomography," *Ophthalmology* **121**, 162–172 (2014).
9. Y. Kanagasingam et al., "Progress on retinal image analysis for age related macular degeneration," *Prog. Retinal Eye Res.* **38**, 20–42 (2014).
10. G. Gregori et al., "Spectral domain optical coherence tomography imaging of drusen in nonexudative age-related macular degeneration," *Ophthalmology* **118**, 1373–1379 (2011).
11. M. A. Sohrab et al., "Image registration and multimodal imaging of reticular pseudodrusen," *Invest. Ophthalmol. Visual Sci.* **52**(8), 5743–5748 (2011).
12. R. P. Finger et al., "Reticular pseudodrusen: a risk factor for geographic atrophy in fellow eyes of individuals with unilateral choroidal neovascularization," *Ophthalmology* **121**, 1252–1256 (2014).
13. M. Marsiglia et al., "Association between geographic atrophy progression and reticular pseudodrusen in eyes with dry age-related macular degeneration," *Invest. Ophthalmol. Visual Sci.* **54**, 7362–7369 (2013).
14. G. Querques et al., "Analysis of progression of reticular pseudodrusen by spectral domain-optical coherence tomography," *Invest Ophthalmol Visual Sci.* **53**(3), 1264–1270 (2012).
15. S. A. Zweifel et al., "Reticular pseudodrusen are subretinal drusenoid deposits," *Ophthalmology* **117**(2), 303–312 (2010).
16. K. Li et al., "Optimal surface segmentation in volumetric images - a graph-theoretic approach," *IEEE Trans. Pattern Anal. Mach. Intell.* **28**, 119–134 (2006).
17. M. K. Garvin et al., "Automated 3D intraretinal layer segmentation of macular spectral-domain optical coherence tomography images," *IEEE Trans. Med. Imaging* **28**, 1436–1447 (2009).
18. Z. Hu et al., "Automated segmentation of the optic disc margin in 3D optical coherence tomography images using a graph-theoretic approach," *Proc. SPIE* **7262**, 72620U (2009).
19. Z. Hu et al., "Multiple layer segmentation and analysis in three-dimensional spectral-domain optical coherence tomography volume scans," *J. Biomed. Opt.* **18**, 076006 (2013).
20. Z. Hu et al., "Semi-automated segmentation of the choroid in spectral-domain optical coherence tomography volume scans," *Invest. Ophthalmol. Visual Sci.* **54**, 1722–1729 (2013).
21. S. J. Chiu et al., "Validated automatic segmentation of AMD pathology including drusen and geographic atrophy in SD-OCT images," *Invest. Ophthalmol. Visual Sci.* **53**, 53–61 (2012).
22. Q. Chen et al., "Automated drusen segmentation and quantification in SD-OCT images," *Med. Image Anal.* **17**, 1058–1072 (2013).
23. S. Lazzeri et al., "Analysis of functional dissociations between best corrected visual acuity and microperimetric parameters in neovascular age-related macular degeneration patients underwent to three monthly ranibizumab injections," *J. Clin. Exp. Ophthalmol.* **4**, 293 (2013).
24. D. J. Rumsey, *Statistics for Dummies*, Wiley, Hoboken, New Jersey (2010).
25. F. L. Ferris et al., "A simplified severity scale for age-related macular degeneration: AREDS report no. 18," *Arch. Ophthalmol.* **123**(11), 1570–1574 (2005).
26. C. Cukras et al., "Natural history of drusenoid pigment epithelial detachment in age-related macular degeneration: age-related eye disease study report no. 28," *Ophthalmology* **117**(3), 489–499 (2010).
27. F. G. Holz et al., "Progression of geographic atrophy and impact of fundus autofluorescence patterns in age-related macular degeneration," *Am. J. Ophthalmol.* **143**(3), 463–472 (2007).
28. C. A. Alexandre Garcia Filho et al., "Spectral-domain optical coherence tomography imaging of drusenoid pigment epithelial detachments," *Retina.* **33**(8), 1558–1566 (2013).
29. R. F. Spaide, "Outer retinal atrophy after regression of subretinal drusenoid deposits as a newly recognized form of late age-related macular degeneration," *Retina* **33**(9), 1800–1808 (2013).

Biographies for the authors are not available.